











Cite this: *J. Mater. Chem. C*, 2023, **11**, 8876

## Cu-modified electrolyte-gated transistors based on reduced graphene oxide†

Rafael Cintra Hensel, <sup>ad</sup> Nicola Comisso, <sup>b</sup> Marco Musiani, <sup>b</sup> Francesco Sedona, <sup>a</sup> Mauro Sambi, <sup>a</sup> Andrea Cester, <sup>c</sup> Nicolò Lago <sup>c</sup> and Stefano Casalini <sup>\*a</sup>

Electrolyte-gated transistors (EGTs) have attracted extensive attention due to their versatility and excellent performance in different fields of electronics. Here, we report on coplanar EGTs based on reduced graphene oxide (rGO), whose gates (flexible Au micro-electrodes) were modified by electrodeposition of either compact or porous Cu coatings (Cu-modified EGTs). The Cu coatings yielded a dramatic change in the minimum gate voltage spanning from  $-50$  mV to  $-300$  mV, which allowed extremely versatile tuning of the device signal. Furthermore, steady measurements led us to carry out prolonged measurements ( $>2$  hours) under a constant bias in NaCl 0.1 M solution which was driven onto the EGTs by using homemade paper fluidics. Transient characterization studies pointed out a potentiometric sensitivity of around 1–3 mV with a signal-to-noise ratio (SNR) close to 5–10 for both electron and hole transport regimes. Since the response time of our Cu-modified EGTs was as low as 80 ms, we succeeded in monitoring emulated action potential (eAP) featuring a characteristic frequency equal to 0.1 Hz.

Received 16th February 2023,  
Accepted 17th May 2023

DOI: 10.1039/d3tc00596h

rsc.li/materials-c

## Introduction

Since the pioneering work of Wrighton *et al.*,<sup>1,2</sup> electrolyte-gated transistors (EGTs) have attracted the attention of many scientists because these electronic devices possess interesting features such as low operational voltages, excellent compliance towards inorganic and organic semiconductors, versatile manufacturing capable of supporting sustainable electronics (*viz.* green and biocompatible electronics), *etc.*<sup>3–16</sup>

In particular, EGTs consist of three terminals (*i.e.*, source, drain and gate electrodes), with a semiconductor material that electrically bridges the drain and source terminals. According to the type of semiconductor, they can be identified as either electrolyte-gated field-effect transistors (EGFETs) or electrochemical transistors (ECTs).<sup>15</sup> Although the boundary between these two classes of devices is rather elusive, the ion penetration into the semiconducting thin film plays a key role, either

triggering faradaic reactions or simply establishing an electrical double-layer.

Several efforts have been made by the scientific community towards three macro-areas:<sup>13–15</sup> (i) an ever-increasing exploration of natural and bio-inspired materials;<sup>4,5,7,17</sup> (ii) the surface engineering of the electro-active interfaces (*viz.* semiconductor/electrolyte, gate/electrolyte *etc.*)<sup>10,13,14,17–21</sup> and (iii) a stepwise sophistication of the device layout.<sup>22–29</sup> For instance, an appealing combination of natural and biocompatible materials such as paper, starch, ethylcellulose and nanoparticle-based ink was demonstrated to fabricate all-printed EGTs that can be possibly transferred to any surface of interest.<sup>5,30–32</sup> Regarding surface engineering, single-molecule detection has been demonstrated by functionalizing the gate terminal with specific antibodies able to detect antigens present in the serum.<sup>33</sup> Another brilliant example is the use of the so-termed extended floating gate architecture introduced by Frisbie *et al.*, who demonstrated the importance of controlling the area of the gate terminal coupled with an additional floating gate to endow EGTs with improved sensing capabilities towards ricin protein.<sup>22</sup>

Here, we focused our efforts on changing the physico-chemical properties of the Au gate surface *via* electrochemical deposition of either compact or compact/porous Cu layers. As a consequence, our method is placed at the border between two out of the three above-mentioned macro-areas, namely surface engineering and layout sophistication. Cu was selected for this study because, although less noble than Au, it is quite stable in

<sup>a</sup> Department of Chemical Sciences (DiSC), University of Padua, via Marzolo 1, 35131, Padua, Italy. E-mail: stefano.casalini@unipd.it

<sup>b</sup> Institute of Condensed Matter Chemistry and Technologies for Energy (ICMATE), National Research Council (CNR), Corso Stati Uniti 4, 35127, Padua, Italy

<sup>c</sup> Department of Information Engineering (DEI), University of Padua, via Gradenigo 6/b, 35131, Padua, Italy

<sup>d</sup> São Carlos Institute of Physics, University of São Paulo, Avenida Trabalhador São Carlense 400, 13566-590, São Carlos, Brazil

† Electronic supplementary information (ESI) available. See DOI: <https://doi.org/10.1039/d3tc00596h>

aqueous media and reliable methods for the deposition of Cu layers with markedly different morphologies are available.<sup>34,35</sup> We show that this approach dramatically changes the EGT performance because the deposition of Cu onto Au affects the work function of the gate terminal<sup>36</sup> and the marked surface roughness factor of the porous Cu layer enhances the capacitance<sup>37</sup> of the interface between an electrolyte and a gate. Compact Cu coatings, with a surface area comparable to that of the pristine Au gate, were obtained by the electrochemical reduction of  $\text{Cu}^{2+}$  ions from concentrated  $\text{CuSO}_4/\text{H}_2\text{SO}_4$  solutions at low current densities. Porous Cu coatings were deposited onto compact ones by hydrogen bubble templated cathodic electrodeposition<sup>38–47</sup> of Cu, a method that allows increase the deposit surface area by at least 100 times.<sup>34,35</sup> A concise description of the main features of hydrogen bubble templated cathodic electrodeposition is provided in the ESI.†

Furthermore, we exploited the features of the Nafion membrane, which is a cation-selective membrane often used in fuel cells.<sup>48–50</sup> Nafion has already been used together with different types of (semi-)conducting materials<sup>51–53</sup> (*viz.* graphene, GO and PEDOT:PSS) without affecting their electronic features, as it offers an additional shield against adventitious contaminants coming from the electrolyte or the outer environment. Since Cu is less noble than Au (*i.e.*, pristine gate terminal), we decided to deposit Nafion also onto the gate terminal, beside the rGO thin film, in order to improve its corrosion resistance. By preventing the transport of aggressive anions towards the Cu surface, Nafion was expected to ensure long-lasting adhesion between Cu and the underlying polycrystalline Au and to improve the EGT stability.

By switching from pristine (*i.e.*, polycrystalline Au gate) to Cu-modified EGTs, we observed a marked shift of the minimum gate voltage (*i.e.*  $-50 \text{ mV} < \Delta V_{\text{G,min}} < -300 \text{ mV}$ ). Such a shift allowed for better tuning of both electron and hole transport with respect to the pristine device. This crucial aspect enables the versatile operation of these devices together with better potentiometric sensitivity. All these beneficial features led us to perform prolonged measurements ( $> 2$  hours of continuous recording) using homemade paper fluidics as well as the real-time monitoring of emulated action potentials (eAPs).

## Experimental section

### Electrodeposition of Cu coatings onto the gate electrode

We fabricated electrolyte-gated rGO thin film transistors on commercially available substrates consisting of Au micro-electrodes sputtered on polyethylene (PET), purchased from Metrohm-Dropsens.<sup>54</sup> These devices comprise Au interdigitated electrodes (IDEs) with a gap of  $30 \mu\text{m}$ , and a coplanar Au square  $3 \times 3 \text{ mm}^2$  gate. A sketch of the system is shown in Fig. 1(a) and (b).

The coplanar Au gate was modified by the electrodeposition of Cu with two distinct morphologies: compact (cCu) and porous (pCu). Electrolyses were performed by using the FET's gate as a cathode and a Pt wire as an anode, both immersed in the electrolytic solutions described below. The solutions,



Fig. 1 (a) Vertical cross-section and (b) top view sketches of the EGT. (c) Sketch and photograph of the paper fluidic setup applied on the Cu-gated devices for long measurements by fluxing  $0.1 \text{ M NaCl}$ .

contained in an undivided glass cell, were vigorously stirred, in contact with the atmosphere and maintained at  $25^\circ\text{C}$  using a thermostat.

A  $0.88 \text{ M CuSO}_4 + 0.55 \text{ M H}_2\text{SO}_4$  solution was used to obtain compact Cu deposits. A constant  $20 \text{ mA cm}^{-2}$  cathodic current density was imposed. By transferring a charge of  $10 \text{ C cm}^{-2}$ , layers with an estimated thickness of  $3.7 \mu\text{m}$  were obtained.

Porous deposits were obtained, on top of the compact ones, using a  $0.05 \text{ M CuSO}_4 + 0.30 \text{ M sodium citrate} + 1.0 \text{ M (NH}_4)_2\text{SO}_4$  solution, at a  $1.0 \text{ A cm}^{-2}$  cathodic current density. This mildly acid solution was preferred to the more often used  $\text{CuSO}_4\text{-H}_2\text{SO}_4\text{-CuCl}_2$  solutions<sup>34</sup> because, when exposed to the latter at an open circuit, the Au source and drain underwent a severe detachment from the plastic substrate. A  $40 \text{ C cm}^{-2}$  charge was transferred. Taking into account the low faradaic efficiency, caused by the concomitant hydrogen evolution, and the apparent density of the porous Cu,<sup>35</sup> the layer thickness was estimated to be around  $15\text{--}20 \mu\text{m}$ .

### Deposition of the rGO-based thin-film

After the cCu- and pCu-based coatings, Au IDEs have been coated by the graphene oxide (GO) thin-film, as shown in Fig. 1(a) and (b). The GO suspension ( $4 \text{ mg mL}^{-1}$ , monolayer content  $> 95\%$ ) was bought from Graphenea, and diluted in the proportion of  $1:10 \text{ v/v}$  in bi-distilled water. For the GO deposition, we exploited the spontaneous adsorption of polyelectrolytes.<sup>55</sup> To promote the adhesion of the polyelectrolytes on top of the device, we used a UV-ozone system for 15 minutes, which produced a negatively charged surface. Thus, as GO is negatively charged, we first immersed the



substrate in a poly(diallylammonium chloride) solution (PDDA, Sigma Aldrich), 1% w/w, and 0.5 M NaCl, for 15 minutes. Then, after a careful rinse with bi-distilled water, we cast a GO droplet (5–10  $\mu\text{l}$ ) onto the IDEs for 3 h. Aiming at blocking the water evaporation, we placed this substrate in a plastic Petri dish containing a water reservoir and sealed it. Finally, we rinsed the samples in bi-distilled water and dried them using a nitrogen stream. For the electrochemical reduction of GO, a droplet of bi-distilled water was placed on top of the samples and grounded using an external Au electrode. The IDEs were short-circuited, and their potential was swept from 0 to  $-3$  V, until achieving the expected grade of GO reduction. Moreover, two different droplets of Nafion 117 ( $\sim 5\%$  in a mixture of lower aliphatic alcohols and water) were spin-coated at 2000 rpm for 1 minute onto the rGO and Cu-modified gate terminals, respectively.

### Electrical and electrochemical characterization

The devices were characterized in bi-distilled water and 0.1 M NaCl. All measurements were performed using a Faraday cage in the dark. An Agilent B1500 parameter analyzer equipped with two high-power and two high-resolution source measurement units (SMUs) was used for the transistor characterization. The  $I$ - $V$  plots adopt the convention introduced by Lago *et al.*<sup>56,57</sup> as it allows an unambiguous description of ambipolar EGTs. The positive (P) and negative (N) terminals act as holes-source/electrons-drain and electrons-source/holes-drain, respectively (*i.e.*,  $V_{\text{P}} \geq 0$  V, and  $V_{\text{N}} < 0$  V).<sup>58</sup> Consequently,  $I_{\text{P}}$  and  $I_{\text{N}}$  are the currents measured through the P and N terminals, which allow us to record rigorously the overall functioning of our device (in our case, the P terminal is always grounded, namely  $V_{\text{P}} = 0$  V).

The electrical characterization of the rGO-based EGTs has been carried out by the data fitting according to eqn (1).

$$I_{\text{PN}} = I_{\text{PNFET}} + \frac{V_{\text{P}} - V_{\text{N}}}{R_{\text{PN}}} \quad (1)$$

where  $R_{\text{PN}}$  is the OFF-state resistance and  $I_{\text{PNFET}}$  is the field-effect current as reported in eqn (S1) in the ESI†. The estimation of the transistor parameter was done by combining the least squares method with the extrapolation procedure reported by P. Servati *et al.*<sup>59</sup> In particular, an initial guess value of  $R_{\text{PN}}$  was estimated from the minimum of the transfer characteristics as  $R_{\text{PN}}^* = V_{\text{PN}}/I_{\text{PNmin}}$ , thus allowing us to compute the field effect current as  $I_{\text{PNFET}}^* = I_{\text{PN}} - V_{\text{PN}}/R_{\text{PN}}^*$ . Then the p- and n-type threshold voltages ( $V_{\text{TP}}$  and  $V_{\text{TN}}$ ), mobility enhancement factors ( $\alpha_{\text{p}}$  and  $\alpha_{\text{n}}$ ), and field-effect mobilities ( $\mu_{\text{FETp}}$  and  $\mu_{\text{FETn}}$ ) were extracted from  $I_{\text{PNFET}}^*$  in unipolar saturation regimes (p- and n-type, respectively) using the method reported in the literature<sup>56,57,59</sup> with eqn (S1) (ESI†). This procedure is then iterated by changing the value of  $R_{\text{PN}}^*$  to minimize the least square error.

To determine the response time, we exploited high  $V_{\text{GP}}$  pulses (*i.e.*,  $V_{\text{GP}} = V_{\text{G}} - V_{\text{P}}$ ,  $\Delta V_{\text{GP}} > 100$  mV), in such a way that the EGT was operated at potentials corresponding to the lowest

and the highest transconductances  $\left(\frac{\partial I_{\text{P}}}{\partial V_{\text{GP}}}\right)$ . To assess the potentiometric sensitivity, we took advantage of rather small  $V_{\text{GP}}$  steps (*i.e.*  $\Delta V_{\text{GP}} < 20$  mV) thereby aiming to define the smallest detectable potential change in the electrolyte.

To characterize the charge/discharge properties of the cCu-modified and pCu-modified EGTs, two kinds of tests were performed, using a Metrohm Autolab Potentiostat-Galvanostat PGSTAT302N. The source and drain electrodes were short-circuited, thereby acting as the counter electrode and the gate as the working electrode. The devices were submitted to standard cycles of charge/discharge by fixing  $I_{\text{charge}} = -I_{\text{discharge}} = 5$   $\mu\text{A}$ . Furthermore, we performed a stepwise protocol composed of the following steps: (i) charging process ( $I_{\text{charge}} = 5$   $\mu\text{A}$ ), (ii) holding state (30 s at  $V_{\text{GP}} = 300$  mV), (iii) open circuit potential (60 s) and (iv) discharging process ( $I_{\text{discharge}} = -5$   $\mu\text{A}$ ).

The eAP recording featured an amplitude of 115 mV<sub>pp</sub> and a frequency of 0.1 Hz using a waveform generator Rigol DG1022. In particular, we superimposed to the gate voltage an eAP based on the Hodgkin–Huxley model.<sup>60</sup>

The prolonged electrical stress was investigated using a lab paper to drive the electrolyte, *i.e.*, 0.1 M NaCl, onto our EGT (see the sketch in Fig. 1(c)). This setup mimics standard fluidics usually built exploiting polymers such as poly(dimethylsiloxane) – PDMS, which allowed us to perform electrical tests lasting some hours without any problems of solvent evaporation. Our characterization relied on recording the current of our EGT as a function of time by fixing  $V_{\text{GP}} = -250$  mV,  $V_{\text{N}} = -300$  mV and  $V_{\text{P}} = 0$  V.

The results shown in the next section were essentially reproduced with at least 5 independent devices.

## Results and discussion

### Preparation and characterization of EGTs with Cu-modified gates

Our EGT relies on the electronic features of rGO, and its manufacturing is completely described elsewhere.<sup>61,62</sup> The main novelties described in this paper are the electrodeposition of Cu onto the planar gate and the use of an additional layer of Nafion cast on top of the rGO-based thin-film and the gate terminal (see Fig. 1(a) and (b)).

The deposition of cCu onto Au gates, according to the procedure described in the experimental section, was straightforward. The optical and SEM images (Fig. S1 in the ESI†) show a continuous and rather smooth Cu deposit. The AFM images (Fig. S2 in the ESI†) show that cCu had an increased roughness with respect to the pristine Au gate, reaching a 208 nm root mean square roughness ( $\sigma_{\text{rms}}$ ), about twice higher than Au. The cCu thickness determined by profilometry was 3.5  $\mu\text{m}$ , a value coherent with that estimated from the electrolysis charge (3.7  $\mu\text{m}$ ).

We encountered severe difficulties (*i.e.* an extensive detachment of the Au deposit from the PET substrate) when we attempted the direct electrodeposition of pCu onto the Au gate



because the required high current density induced delamination of the Au layers from the underlying PET substrate. However, we succeeded in depositing pCu on top of the compact layer, thus obtaining the pCu-modified gates described below. Details of the electrodeposition of pCu onto FET gates are described in the ESI†

The SEM images of pCu deposits show a macroporous structure similar but not identical to those observed when electrodeposition was performed from  $\text{CuSO}_4/\text{H}_2\text{SO}_4/\text{CuCl}_2$  solutions on bulky electrodes.<sup>35,47</sup> The large pores are less deep and cover the electrode surface less homogeneously. However, the higher magnification images (Fig. S3(a)–(c), ESI†) prove that the Cu deposit obtained from the sulfate-citrate medium consists of an assembly of nanowires, ensuring porosity on the nanometric scale and a large surface roughness factor. To explain fine morphological differences, it is worth observing that the Cu deposition mechanism may not be identical in sulfate-citrate solution and sulfate-chloride solution, due to differences in their initial pH values (*ca.* 5 and below 1, respectively). In the former, under vigorous hydrogen evolution, the local pH increases and so, besides being directly reduced to Cu,  $\text{Cu}^{2+}$  may undergo hydrolysis to form CuO, eventually reduced to Cu. Probably, markedly different hydrodynamic conditions, which strongly influenced  $\text{H}_2$  bubble release, also contributed to determining morphological differences. The pCu deposit thickness assessed by profilometry was 20  $\mu\text{m}$ . Its mean square roughness could not be determined, as it was well above the upper limit measurable by AFM.

The final step consisted of depositing the GO-based thin film onto the IDEs together with its electrochemical reduction to achieve the rGO.

### I–V transfer characteristics

Electrical characterization has been performed by recording standard *I*–*V* transfer characteristics in both Milli-Q water (Fig. 2) and 0.1 M NaCl (Fig. S4 in the ESI†), because the former gives preliminary clues on the Cu-modified EGT performance, whereas the latter provides relevant information on their operation in more demanding environments, similar to real matrixes. Although the standard convention is well-established for both unipolar and ambipolar transistors, we adopted a specific convention recently proposed by N. Lago *et al.*<sup>56,57</sup> in order to define unambiguously the injection/collection of electrons/holes in our ambipolar EGTs based on rGO.

Fig. 2(a)–(c) show the *I*–*V* transfer characteristics obtained in Milli-Q water for pristine, cCu-, and pCu-modified EGTs, in which  $V_N = -300$  mV and  $V_P = 0$  V (*i.e.*, the common terminal for both gate and N terminals), and the gate potential  $V_{GP}$  was swept from  $-300$  mV to  $+300$  mV. Albeit the ambipolar behaviour of graphene and its derivatives is known, the pristine Au gate transistor shows mainly hole conduction. This trend agrees with previous flexible EGTs featuring a coplanar liquid gate.<sup>62</sup> cCu- and pCu-modified EGTs show the improved conduction of the electrons/holes. Both conduction branches (*viz.* p- and n-type regimes) are clearly defined due to the dramatic change of  $V_{G,\min}$  (*i.e.*  $-50$  mV  $< \Delta V_{G,\min} < -100$  mV). This negative  $V_{G,\min}$  shift (*i.e.*, negative doping) strengthens the

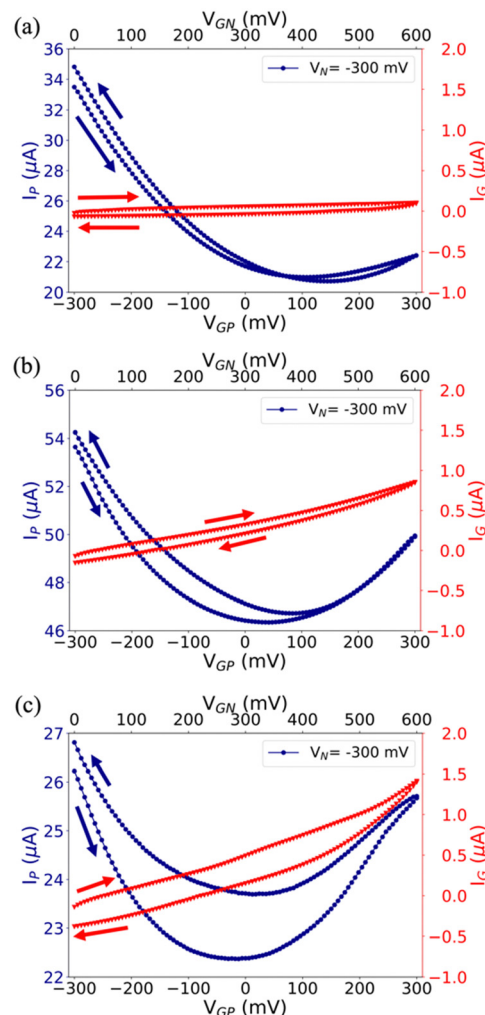


Fig. 2 *I*–*V* transfer characteristics of the rGO device featuring the (a) pristine Au, (b) cCu-modified Au gate, (c) pCu-modified Au gate recorded in Milli-Q water. The red curve stands for the leakage current ( $I_G$ ) and the blue one stands for the current recorded at the P terminal ( $I_P$ ).  $V_P = 0$  V and  $V_N = -300$  mV.  $V_{GP}$  and  $V_{GN} = (V_G - V_N)$  ranges are presented as the bottom and top x-axis, respectively.

electron conduction compared to the pristine EGT and may be ascribed to the change in the gate work function, as already observed by Kergoat *et al.*<sup>36</sup> Further proof of the better performance of the Cu-modified EGTs than the reference one is the appropriate control of  $V_{G,\min}$  according to the  $V_N$  variation (Fig. S5a–c in the ESI†).<sup>58</sup> Coherently to these observations, the use of 0.1 M NaCl causes a relevant shift in the operational voltages of Cu-modified gate devices, whereas the pristine Au gate device is unaffected, as a result of its poor electronic modulation (see Fig. S4, ESI†). Comparing pristine EGTs with cCu/pCu-modified ones,  $\Delta V_{G,\min}$  is also amplified with respect to bi-distilled water, spanning from  $-200$  mV to  $-300$  mV. Among the possible reasons for this change in performance between bi-distilled water and 0.1 M NaCl, one of the most relevant is the more efficient electrostatic screening of mobile or fixed charges around the conductive channel of the EGT, since electrostatic





screening is strictly related to the Debye length (*i.e.* a shortening of the Debye length at a higher ionic strength).<sup>63</sup> According to the  $I$ - $V$  transfer characteristics, the mobility and threshold voltages of holes ( $\mu_h$ ,  $V_{th,p}$ ) and electrons ( $\mu_e$ ,  $V_{th,n}$ ) have been calculated by using eqn (S1) (ESI†) which describes ambipolar transistors, as reported elsewhere.<sup>56,57</sup> Our data (Table S1, ESI†) provide an accurate characterization of these EGTs by changing systematically the electrolyte (bi-distilled water *vs.* 0.1 M NaCl) and the values of  $V_N$ .

### Investigation of transient phenomena

To achieve a more comprehensive view of the performance of Cu-modified EGTs, we performed a further investigation on transient phenomena such as the response time, potentiometric sensitivity, and capability to store/deliver charge. These technological issues are pivotal for the development of electronic devices operated like transducers capable of recording biological/bio-physical events (*e.g.*, antibody-antigen pairing, neuronal spikes, heartbeats, and the release of drugs).<sup>64–69</sup>

We determined the response time and potentiometric sensitivity of EGTs by recording  $I_p$  as a function of time, in response to  $V_{GP}$  pulses of variable magnitude, by using 0.1 M NaCl as the electrolyte. Fig. 3(a) and Fig. S6 in the ESI† (relevant to p- and n-type conduction, respectively) show that the experimental  $I_p$  decay may be accurately fit by using eqn (2) which

exploits the sum of two exponentials.

$$I(t) = A + B \times \exp(-t/\tau_1) + C \times \exp(-t/\tau_2) \quad (2)$$

where  $A$ ,  $B$ ,  $C$ ,  $\tau_1$ , and  $\tau_2$  are the functions of resistances, capacitances, steady-state drain current, gate voltage and transconductance, according to the equivalent circuit proposed elsewhere.<sup>70</sup> This equation was already exploited for electrochemical organic transistors featuring a membrane onto the active material, where  $\tau_1 > \tau_2$ .<sup>64</sup> In particular,  $\tau_1$  refers to the charging time of the active material, and  $\tau_2$  refers to the charging time of the membrane cast on top of it. In our case, this model can be applied by attributing  $\tau_1$  to the rGO charging process, and  $\tau_2$  to that of Nafion. Considering the experimental curve shown in Fig. 3(a), we obtained  $\tau_1 = 26 \pm 1$  s and  $\tau_2 = 0.08 \pm 0.01$  s.

Regarding the potentiometric sensitivity, Fig. 3(b) and Fig. S7 (ESI†) show that pCu-modified EGTs are the most sensitive because they reach the highest signal-to-noise ratio (SNR), *i.e.*, 5.8 and 12, for the p- and n-branches, respectively, and the lowest recordable  $V_{GP}$  step, namely 1 mV and 3 mV for holes and electrons, respectively (see Table S2, ESI†). This can be ascribed to the increased roughness of the pCu coating with respect to both the pristine Au and cCu gate terminals. This leads to a more efficient electrical double layer at the gate

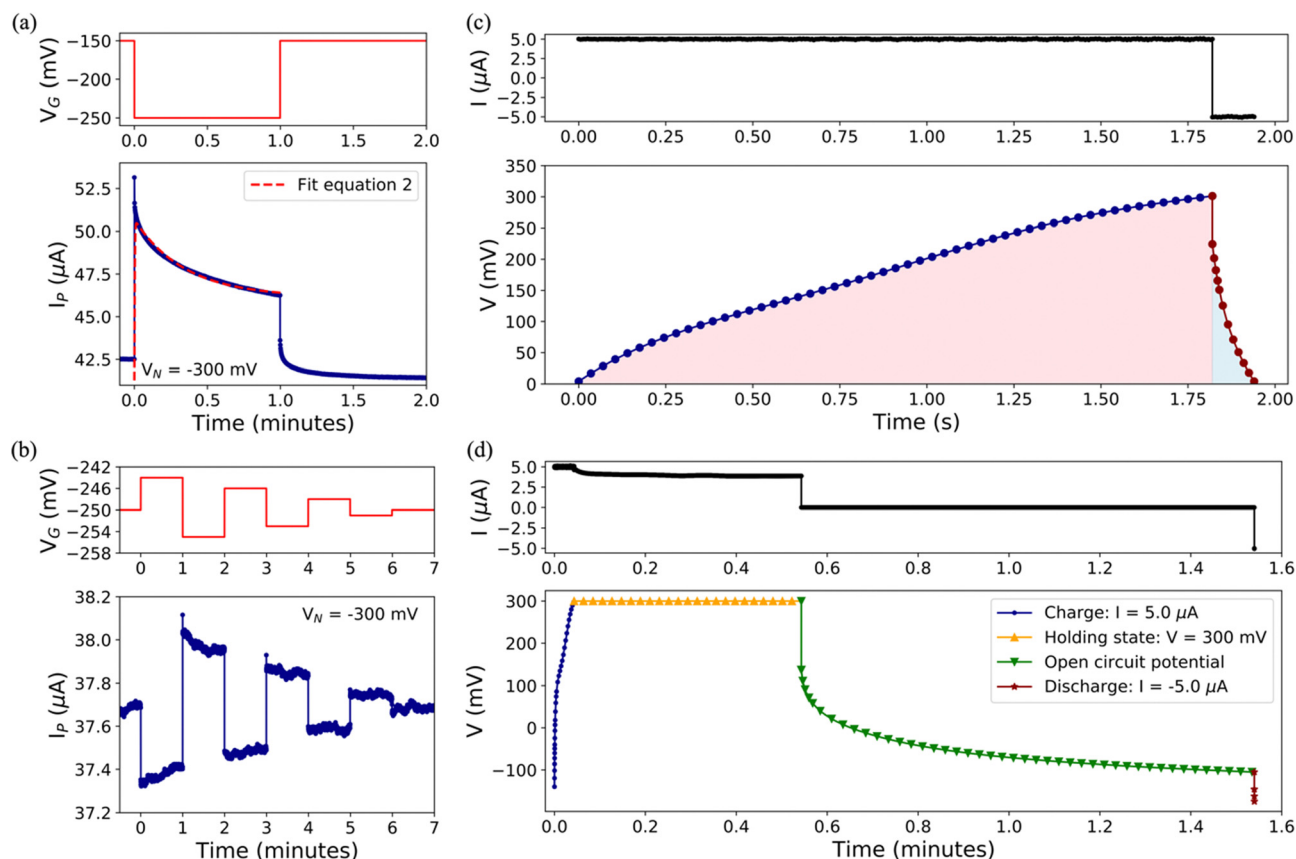


Fig. 3 (a) Response time (the red dashed line is the fit), (b) potentiometric sensitivity and (c) and (d) galvanostatic charge/discharge of the pCu-gated EGT. All measurements are performed in NaCl 0.1 M.



interface, which enhances the amplification feature of the pCu-modified EGT.

Aiming at gaining more insights into the role played by Cu related to these performances, we performed standard cycles of charge/discharge with  $I_{\text{charge}} = -I_{\text{discharge}} = 5 \mu\text{A}$ , which is a standard value of the leakage current (*viz.*  $I_G$ ). The non-linear trend hints at pseudo-capacitor behaviour, instead of a simple capacitor, for both pCu- (Fig. 3(c)) and cCu-based (Fig. S8, ESI†) coatings.<sup>71</sup> The coulombic efficiency (*viz.*  $Q_{\text{discharge}}/Q_{\text{charge}}$ ) was higher for pCu (7.7%) than that for cCu (5.4%), due to its pronounced porosity and true surface area. Further tests have been carried out according to the protocol described in the Experimental section, which involved a holding step at a constant  $V_{\text{GP}} = 300 \text{ mV}$  and an open circuit step between the charging and discharging steps, allowing us to highlight the different efficiencies for cCu and pCu. The leakage current at a fixed  $V_{\text{GP}}$  was more pronounced for cCu than pCu, decreasing

from  $5 \mu\text{A}$  to  $2.9 \mu\text{A}$  and  $3.9 \mu\text{A}$ , respectively. During the open circuit step, the decrease of the voltage was faster for cCu than pCu (further details in the ESI†). Moreover, the charge/discharge protocol allowed us to extract energy and power involved in the device's functioning (see Table S2, ESI†).

### Recording of the emulated action potential and response to prolonged electrical stress

Aiming at more technologically relevant applications, we submitted our EGTs towards two tests: (i) recording of the emulated action potential (eAP) and (ii) prolonged electrical monitoring. Other types of (semi-)conducting materials,<sup>64,65,72,73</sup> implemented in the EGT layout succeeded towards the real-time monitoring of biological signalling. According to the  $V_{\text{GP}}$  set point (*i.e.*,  $+250 \text{ mV}$  and  $-250 \text{ mV}$ ) of the eAP, the user can select the n- or p-type conduction (see Fig. S9, ESI†). The former shows an increase in  $I_P$  related to the eAP; in contrast, the latter shows an  $I_P$  decrease (see Fig. 4). As a result, the pCu-modified EGT succeeded in recording the eAP for both types of conduction, whereas the cCu-modified one showed only a partial recording for p-type conduction (see Fig. S10, ESI†), which is coherent with the potentiometric sensitivity previously shown (see Fig. S7d, ESI†).

The prolonged electrical monitoring shows that  $I_P$  decreases over time following two distinct processes: (i) one faster within 50 s, and (ii) another slower for the rest of the measurement, as depicted in Fig. 5, until  $I_P$  stabilizes at  $\sim 36.7 \mu\text{A}$ , after 2 hours. Such long-term measurement is an important issue to consider towards the real-time monitoring of a particular environment for biological and chemical purposes. A fingerprint for the stable functioning of the device even after prolonged tests ( $> 2$  hours) is the conservation of almost identical  $I$ - $V$  transfer characteristics as shown in Fig. S11 (ESI†). We can safely rule out any faradaic reaction that might damage the device. Similar behaviour has been observed for the cCu-modified

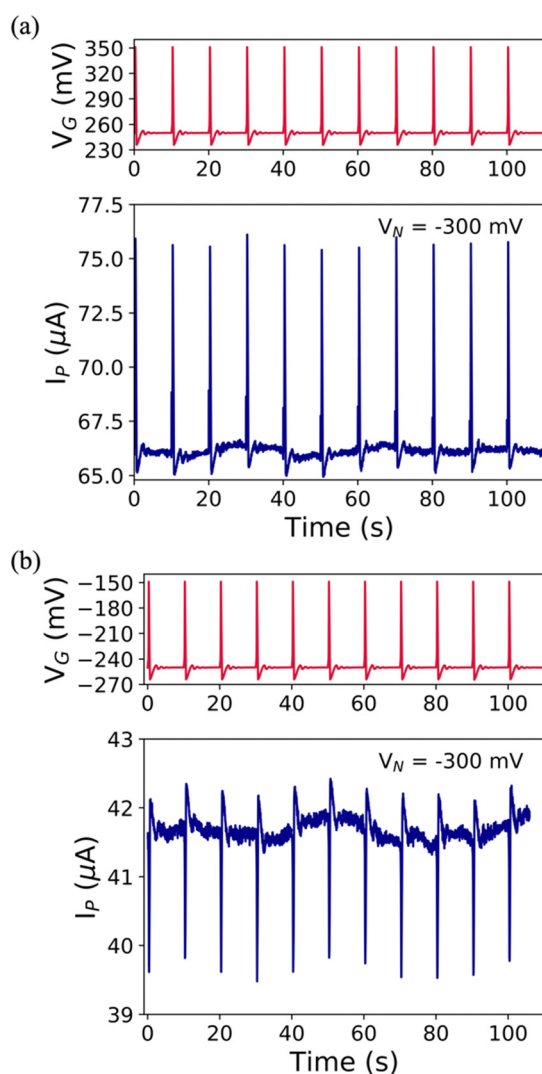


Fig. 4 Emulated AP iterative series (red lines) and its recorded AP iterative series (blue lines) featuring (a)  $+250 \text{ mV}$  set point potential and (b)  $-250 \text{ mV}$  set point potential in NaCl 0.1 M.

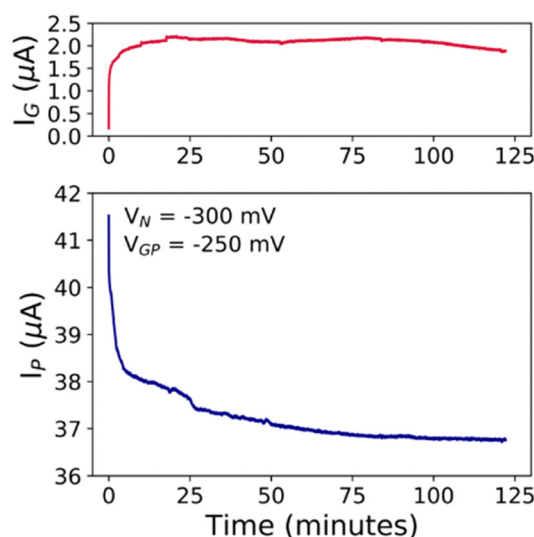


Fig. 5 (a)  $I_G$  and (b)  $I_P$  vs. time plots for the prolonged electrical stress investigation, in which  $V_N = -300 \text{ mV}$  and  $V_{\text{GP}} = -250 \text{ mV}$  were fixed in 0.1 M NaCl.



EGT operated under the same conditions (compare Fig. S12 in the ESI† with Fig. 5). In particular, these devices succeeded only by using  $V_{GP} < 0$  V (*viz.* hole conduction), because  $V_{GP} > 0$  V triggers the partial oxidation of the electrodeposited Cu, and its consequent electromigration onto the rGO thin film during prolonged measurements, thereby damaging the device.

## Conclusions

In this paper, we demonstrated how it is possible to couple the fabrication of an EGT based on the rGO thin film with the electrodeposition of Cu onto the ultrathin (*viz.* 20 nm thick) coplanar gate terminal. Two types of Cu coatings can be achieved: a compact (cCu) coating with a morphology resembling that of the underlying polycrystalline Au, and a porous (pCu) one, whose morphology shows a dual porosity. The Cu modification of the gate terminal shows the relevant n-doping of these EGTs, namely  $-50 \text{ mV} < \Delta V_{G,\min} < -300 \text{ mV}$  according to different electrolytes and operational voltages. This allows extreme versatility in the Cu-modified EGT operation. As a result, we succeeded in operating the device in NaCl 0.1 M, which has an ionic strength comparable to real matrixes such as tap water, seawater and biological fluids. Moreover, the pCu-modified EGT showed a potentiometric sensitivity down to 1–3 mV for p- and n-type conduction, respectively, in a time scale of  $< 1$  s and a SNR of  $\cong 6$ –10. For these reasons, it has been possible to track emulated action potentials (eAPs) with a characteristic frequency of 0.1 Hz. Prolonged tests ( $> 2$  hours) carried out using home-made paper fluidics showed satisfactory stability without any significant damage. These promising outcomes offer a new perspective in terms of the surface engineering and layout sophistication of such EGTs, paving the way towards novel sensors and/or transducers.

## Author contributions

Rafael Cintra Hensel: data curation, formal analysis, investigation, validation, software, visualization, writing – original draft, and writing – review and editing. Nicola Comisso: investigation and data curation. Marco Musiani: resources and writing – review and editing. Francesco Sedona: resources and writing – review and editing. Mauro Sambi: resources, writing – review and editing, and funding acquisition. Andrea Cester: resources and writing – review and editing. Nicolò Lago: investigation, formal analysis, and software. Stefano Casalini: conceptualization, funding acquisition, investigation, methodology, project administration, resources, supervision, validation, writing – original draft, and writing – review and editing.

## Conflicts of interest

There are no conflicts to declare.

## Acknowledgements

The authors acknowledge the financial support from the Italian Ministry of Education, Universities, and Research through the project “Nanochemistry for Energy and Health, Nexus” – the national funding network termed “Dipartimenti di Eccellenza” awarded to the Department of Chemical Sciences at the University of Padua and the project P-DiSC#11Nexus\_BIRD2020-UNIPD (CARBON-FET) led by Prof. Stefano Casalini. RCH acknowledges the research grant no. 2020/15095-0 from São Paulo Research Foundation - FAPESP (Brazil).

## References

- 1 H. S. White, G. P. Kittleson and M. S. Wrighton, *J. Am. Chem. Soc.*, 1984, **106**, 5375–5377.
- 2 E. W. Paul, A. J. Ricco and M. S. Wrighton, *J. Phys. Chem.*, 1985, **89**, 1441–1447.
- 3 M. Irimia-Vladu, *Chem. Soc. Rev.*, 2014, **43**, 588–610.
- 4 A. S. Sharova and M. Caironi, *Adv. Mater.*, 2021, **33**, 2103183.
- 5 G. E. Bonacchini, C. Bossio, F. Greco, V. Mattoli, Y.-H. Kim, G. Lanzani and M. Caironi, *Adv. Mater.*, 2018, **30**, 1706091.
- 6 M. Irimia-Vladu, E. D. Głowacki, G. Voss, S. Bauer and N. S. Sariciftci, *Mater. Today*, 2012, **15**, 340–346.
- 7 A. S. Sharova, F. Melloni, G. Lanzani, C. J. Bettinger and M. Caironi, *Adv. Mater. Technol.*, 2021, **6**, 2000757.
- 8 M. Irimia-Vladu, P. A. Troshin, M. Reisinger, L. Shmygleva, Y. Kanbur, G. Schwabegger, M. Bodea, R. Schwödiauer, A. Mumyatov, J. W. Fergus, V. F. Razumov, H. Sitter, N. S. Sariciftci and S. Bauer, *Adv. Funct. Mater.*, 2010, **20**, 4069–4076.
- 9 C. Sun, X. Liu, Q. Jiang, X. Ye, X. Zhu and R.-W. Li, *Sci. Technol. Adv. Mater.*, 2023, **24**, 2162325.
- 10 G. Y. Wang, K. Lian and T.-Y. Chu, *IEEE J. Electron Devices Soc.*, 2021, **9**, 939–950.
- 11 B. Shkodra, M. Petrelli, M. A. Costa Angeli, D. Garoli, N. Nakatsuka, P. Lugli and L. Petti, *Appl. Phys. Rev.*, 2021, **8**, 041325.
- 12 H. Ling, D. A. Koutsouras, S. Kazemzadeh, Y. van de Burgt, F. Yan and P. Gkoupidenis, *Appl. Phys. Rev.*, 2020, **7**, 011307.
- 13 F. Torricelli, D. Z. Adrahtas, Z. Bao, M. Berggren, F. Biscarini, A. Bonfiglio, C. A. Bortolotti, C. D. Frisbie, E. Macchia, G. G. Malliaras, I. McCulloch, M. Moser, T.-Q. Nguyen, R. M. Owens, A. Salleo, A. Spanu and L. Torsi, *Nat. Rev. Methods Primers*, 2021, **1**, 66.
- 14 W. Huang, J. Chen, G. Wang, Y. Yao, X. Zhuang, R. M. Pankow, Y. Cheng, T. J. Marks and A. Facchetti, *J. Mater. Chem. C*, 2021, **9**, 9348–9376.
- 15 S. H. Kim, K. Hong, W. Xie, K. H. Lee, S. Zhang, T. P. Lodge and C. D. Frisbie, *Adv. Mater.*, 2013, **25**, 1822–1846.
- 16 S. Nandy, S. Goswami, A. Marques, D. Gaspar, P. Grey, I. Cunha, D. Nunes, A. Pimentel, R. Igreja, P. Barquinha, L. Pereira, E. Fortunato and R. Martins, *Adv. Mater. Technol.*, 2021, **6**, 2000994.



- 17 I. Cunha, R. Barras, P. Grey, D. Gaspar, E. Fortunato, R. Martins and L. Pereira, *Adv. Funct. Mater.*, 2017, **27**, 1606755.
- 18 M. Berto, C. Diacci, R. D'Agata, M. Pinti, E. Bianchini, M. Di Lauro, S. Casalini, A. Cossarizza, M. Berggren, D. Simon, G. Spoto, F. Biscarini and C. A. Bortolotti, *Adv. Biosyst.*, 2018, **2**, 1700072.
- 19 S. Casalini, F. Leonardi, T. Cramer and F. Biscarini, *Org. Electron.*, 2013, **14**, 156–163.
- 20 M. S. Thomas, S. P. White, K. D. Dorfman and C. D. Frisbie, *J. Phys. Chem. Lett.*, 2018, **9**, 1335–1339.
- 21 Y. S. Rim, H. Chen, B. Zhu, S.-H. Bae, S. Zhu, P. J. Li, I. C. Wang and Y. Yang, *Adv. Mater. Interfaces*, 2017, **4**, 1700020.
- 22 S. P. White, S. Sreevatsan, C. D. Frisbie and K. D. Dorfman, *ACS Sens.*, 2016, **1**, 1213–1216.
- 23 S. P. White, K. D. Dorfman and C. D. Frisbie, *Anal. Chem.*, 2015, **87**, 1861–1866.
- 24 S. P. White, K. D. Dorfman and C. D. Frisbie, *J. Phys. Chem. C*, 2016, **120**, 108–117.
- 25 K. Fukuda, T. Minamiki, T. Minami, M. Watanabe, T. Fukuda, D. Kumaki and S. Tokito, *Adv. Electron. Mater.*, 2015, **1**, 1400052.
- 26 M. S. Ozório, D. H. Vieira, G. L. Nogueira, C. S. Martin, N. Alves and C. J. L. Constantino, *Mater. Sci. Semicond. Process.*, 2022, **151**, 107045.
- 27 M. Nikolka, D. Simatos, A. Foudeh, R. Pfattner, I. McCulloch and Z. Bao, *ACS Appl. Mater. Interfaces*, 2020, **12**, 40581–40589.
- 28 D. Gaspar, J. Martins, P. Bahubalindruni, L. Pereira, E. Fortunato and R. Martins, *Adv. Electron. Mater.*, 2018, **4**, 1800423.
- 29 R. Morais, D. H. Vieira, M. dos, S. Klem, C. Gaspar, L. Pereira, R. Martins and N. Alves, *Semicond. Sci. Technol.*, 2022, **37**, 035007.
- 30 L. Santos, D. Nunes, T. Calmeiro, R. Branquinho, D. Salgueiro, P. Barquinha, L. Pereira, R. Martins and E. Fortunato, *ACS Appl. Mater. Interfaces*, 2015, **7**, 638–646.
- 31 J. T. Carvalho, V. Dubceac, P. Grey, I. Cunha, E. Fortunato, R. Martins, A. Clausner, E. Zschech and L. Pereira, *Nanomaterials*, 2019, **9**(2), 169.
- 32 P. I. C. Claro, I. Cunha, R. T. Paschoalin, D. Gaspar, K. Miranda, O. N. Oliveira Jr., R. Martins, L. Pereira, J. M. Marconcini, E. Fortunato and L. H. C. Mattoso, *ACS Appl. Mater. Interfaces*, 2021, **13**, 26237–26246.
- 33 E. Macchia, K. Manoli, B. Holzer, C. Di Franco, M. Ghittorelli, F. Torricelli, D. Alberga, G. F. Mangiatordi, G. Palazzo, G. Scamarcio and L. Torsi, *Nat. Commun.*, 2018, **9**, 3223.
- 34 N. Comisso, S. Cattarin, P. Guerriero, L. Mattarozzi, M. Musiani, L. Vázquez-Gómez and E. Verlato, *J. Solid State Electrochem.*, 2016, **20**, 1139–1148.
- 35 L. Mattarozzi, S. Cattarin, N. Comisso, A. Gambirasi, P. Guerriero, M. Musiani, L. Vazquez Gomez and E. Verlato, *Electrochim. Acta*, 2014, **140**, 337–344.
- 36 L. Kergoat, L. Herlogsson, B. Piro, M. C. Pham, G. Horowitz, X. Crispin and M. Berggren, *Proc. Natl. Acad. Sci. U. S. A.*, 2012, **109**, 8394–8399.
- 37 M. Singh, K. Manoli, A. Tiwari, T. Ligonzo, C. Di Franco, N. Cioffi, G. Palazzo, G. Scamarcio and L. Torsi, *J. Mater. Chem. C*, 2017, **5**, 3509–3518.
- 38 H.-C. Shin, J. Dong and M. Liu, *Adv. Mater.*, 2003, **15**, 1610–1614.
- 39 H.-C. Shin and M. Liu, *Chem. Mater.*, 2004, **16**, 5460–5464.
- 40 N. D. Nikolić and K. I. Popov, in *Electrodeposition: Theory and Practice*, ed. S. S. Djokic, Springer, New York, NY, 2010, pp. 1–70.
- 41 Y. Li, W.-Z. Jia, Y.-Y. Song and X.-H. Xia, *Chem. Mater.*, 2007, **19**, 5758–5764.
- 42 D. Nam, R. Kim, D. Han, J. Kim and H. Kwon, *Electrochim. Acta*, 2011, **56**, 9397–9405.
- 43 S. Cherevko, X. Xing and C.-H. Chung, *Electrochem. Commun.*, 2010, **12**, 467–470.
- 44 S. Cherevko and C.-H. Chung, *Electrochim. Acta*, 2010, **55**, 6383–6390.
- 45 S. Cherevko and C.-H. Chung, *Electrochem. Commun.*, 2011, **13**, 16–19.
- 46 S. Cherevko, X. Xing and C.-H. Chung, *Appl. Surf. Sci.*, 2011, **257**, 8054–8061.
- 47 L. Mattarozzi, S. Cattarin, N. Comisso, P. Guerriero, M. Musiani and E. Verlato, *Electrochim. Acta*, 2016, **198**, 296–303.
- 48 M. B. Karimi, F. Mohammadi and K. Hooshyari, *Int. J. Hydrogen Energy*, 2019, **44**, 28919–28938.
- 49 X. Shi, Y. Ma, X. Huo, O. C. Esan and L. An, *Int. J. Green Energy*, 2021, 1–7.
- 50 F. A. Zakil, S. K. Kamarudin and S. Basri, *Renewable Sustainable Energy Rev.*, 2016, **65**, 841–852.
- 51 Z. Wang, Z. Hao, X. Wang, C. Huang, Q. Lin, X. Zhao and Y. Pan, *Adv. Funct. Mater.*, 2021, **31**, 2005958.
- 52 S. J. Lue, Y.-L. Pai, C.-M. Shih, M.-C. Wu and S.-M. Lai, *J. Membr. Sci.*, 2015, **493**, 212–223.
- 53 P.-P. Lu, D.-S. Shang, C.-S. Yang and Y. Sun, *J. Phys. D: Appl. Phys.*, 2020, **53**, 485102.
- 54 Flexible Gold Field-Effect Transistors with coplanar gate, [https://www.dropsens.com/en/pdfs\\_productos/new\\_brochures/aufet30.pdf](https://www.dropsens.com/en/pdfs_productos/new_brochures/aufet30.pdf), (accessed 9 February 2023).
- 55 G. Decher, *Science*, 1979, **199**(277), 1232–1237.
- 56 N. Lago, M. Buonomo, R. C. Hensel, F. Sedona, M. Sambì, S. Casalini and A. Cester, *IEEE Trans. Electron Devices*, 2022, **69**, 3192–3198.
- 57 N. Lago, M. Buonomo, R. C. Hensel, F. Sedona, M. Sambì, S. Casalini and A. Cester, *IEEE Trans. Electron Devices*, 2022, **69**, 6492.
- 58 S. Lee, A. Nathan, J. Alexander-Webber, P. Braeuninger-Weimer, A. A. Sagade, H. Lu, D. Hasko, J. Robertson and S. Hofmann, *ACS Appl. Mater. Interfaces*, 2018, **10**, 10618–10621.
- 59 P. Servati, D. Striakhilev and A. Nathan, *IEEE Trans. Electron Devices*, 2003, **50**, 2227–2235.
- 60 A. L. Hodgkin and A. F. Huxley, *J. Physiol.*, 1952, **117**, 500–544.
- 61 R. Furlan de Oliveira, V. Montes-García, P. A. Livio, M. B. González-García, P. Fanjul-Bolado, S. Casalini and P. Samorì, *Small*, 2022, **18**, 2201861.
- 62 R. Furlan de Oliveira, P. A. Livio, V. Montes-García, S. Ippolito, M. Eredia, P. Fanjul-Bolado, M. B. González García, S. Casalini and P. Samorì, *Adv. Funct. Mater.*, 2019, **29**(46), 1905375.





- 63 T. Xiao and X. Song, *J. Chem. Phys.*, 2011, **135**, 104104.
- 64 A. Campana, T. Cramer, D. T. Simon, M. Berggren and F. Biscarini, *Adv. Mater.*, 2014, **26**, 3874–3878.
- 65 T. Cramer, B. Chelli, M. Murgia, M. Barbalinardo, E. Bystrenova, D. M. de Leeuw and F. Biscarini, *Phys. Chem. Chem. Phys.*, 2013, **15**, 3897–3905.
- 66 S. Casalini, A. C. Dumitru, F. Leonardi, C. A. Bortolotti, E. T. Herruzo, A. Campana, R. F. de Oliveira, T. Cramer, R. Garcia and F. Biscarini, *ACS Nano*, 2015, **9**, 5051–5062.
- 67 R. A. Picca, K. Manoli, E. Macchia, L. Sarcina, C. Di Franco, N. Cioffi, D. Blasi, R. Österbacka, F. Torricelli, G. Scamarcio and L. Torsi, *Adv. Funct. Mater.*, 2020, **30**, 1904513.
- 68 E. Macchia, R. A. Picca, K. Manoli, C. Di Franco, D. Blasi, L. Sarcina, N. Ditaranto, N. Cioffi, R. Österbacka, G. Scamarcio, F. Torricelli and L. Torsi, *Mater. Horiz.*, 2020, **7**, 999–1013.
- 69 G. Foschi, F. Leonardi, A. Scala, F. Biscarini, A. Kovtun, A. Liscio, A. Mazzaglia and S. Casalini, *Nanoscale*, 2015, **7**, 20025–20032.
- 70 G. C. Faria, D. T. Duong and A. Salleo, *Org. Electron.*, 2017, **45**, 215–221.
- 71 T. S. Mathis, N. Kurra, X. Wang, D. Pinto, P. Simon and Y. Gogotsi, *Adv. Energy Mater.*, 2019, **9**, 1902007.
- 72 L. H. Hess, M. Jansen, V. Maybeck, M. V. Hauf, M. Seifert, M. Stutzmann, I. D. Sharp, A. Offenhäusser and J. A. Garrido, *Adv. Mater.*, 2011, **23**, 5045–5049.
- 73 A. Kyndiah, F. Leonardi, C. Tarantino, T. Cramer, R. Millan-Solsona, E. Garreta, N. Montserrat, M. Mas-Torrent and G. Gomila, *Biosens. Bioelectron.*, 2020, **150**, 111844.

